Emerging microfluidic devices for cancer cells/biomarkers manipulation and detection

Victor Hugo Perez-Gonzalez[1], Roberto Carlos Gallo-Villanueva[1], Sergio Camacho-Leon[1], Jose Isabel Gomez-Quiñones[2], Jose Manuel Rodriguez-Delgado[1], Sergio Omar Martinez-Chapa[1] ✉

[1]School of Engineering and Sciences, Tecnologico de Monterrey, Avenue Eugenio Garza Sada 2501 Sur, Monterrey, Mexico
[2]School of Biotechnology and Health Sciences, Tecnologico de Monterrey, Avenue Eugenio Garza Sada 2501 Sur, Monterrey, Mexico
✉ E-mail: smart@itesm.mx

Abstract: Circulating tumour cells (CTCs) are active participants in the metastasis process and account for ~90% of all cancer deaths. As CTCs are admixed with a very large amount of erythrocytes, leukocytes, and platelets in blood, CTCs are very rare, making their isolation, capture, and detection a major technological challenge. Microfluidic technologies have opened-up new opportunities for the screening of blood samples and the detection of CTCs or other important cancer biomarker-proteins. In this study, the authors have reviewed the most recent developments in microfluidic devices for cells/biomarkers manipulation and detection, focusing their attention on immunomagnetic-affinity-based devices, dielectrophoresis-based devices, surface-plasmon-resonance microfluidic sensors, and quantum-dots-based sensors.

1 Introduction

Approximately 90% of all cancer deaths are caused by the cell metastasis process. Unfortunately, from all cancer processes, cancer cell metastasis is the least understood aspect of the disease [1]. Nevertheless, some insights are available in reference to the sequence of steps followed by cancer cells in order to invade and colonise organs distant from their primary tumour site. First, as the normal oxygen supply is insufficient to meet the requirements of cancer cells, the angiogenesis process is activated. At the same time, downregulation of adhesion molecules leads to invasion of surrounding stroma and intravasation of tumour cells resistant to apoptosis. While invading the vessels, they undergo the epithelial-to-mesenchymal transition process, which confers to them the traits of tumour-initiating, self-renewal, and spawn-progeny potential, motility, and invasiveness. Tumour cells travel through the circulatory system to distant organs, though, mainly because of their size, many of them are destroyed or damaged in the circulation as they cannot pass through the bores of capillaries. The few undamaged tumour cells may extravasate, invading the parenchyma of foreign tissue. However, most of these do not survive the response from the innate immune system. Nonetheless, few of them may survive, adapt, and proliferate, colonising the organ and creating a new carcinoma, as shown in Fig. 1 [2].

Cells that travel through the circulatory system are referred to as circulating tumour cells (CTCs) and are extremely rare. On average, 5×10^9 erythrocytes, 7.8×10^6 leukocytes, and 3.5×10^8 platelets are present in 1 ml of blood. CTCs, when present, do not exceed 100 cells/ml [3]. Hence, detecting these cells while keeping them viable to perform subsequent analysis (e.g. employing cellular, microscopic, or molecular techniques) is of utmost importance in order to find the most effective therapy to prevent further proliferation of the disease. Several different biomarkers (i.e. proteins), in addition to CTCs, are present in blood and in other human fluids such as serum and urine when the patient has developed cancer. Therefore, these can also be employed to detect the presence of cancer at early stages and prevent further proliferation of the disease [4].

Microfluidics emerged from the micro-electro-mechanical systems (MEMS) field as a multidisciplinary research line devoted to study the behaviour of fluids constrained in micrometre-sized channels [5]. Fluidic channels with such small dimensions have been proven to be effective for a number of applications, for example, to perform precise measurements and assays for drug screening, enzymatic reactions and nucleic acid amplification [1]. Many microfluidic devices have been recently developed to manipulate or detect cancer cells and biomarkers. Owing to the vast range of available manipulation or detection mechanisms, it is important to classify microfluidic devices into several groups according to their operating principle. For example, it is possible to develop devices in which electric, magnetic, acoustic, centrifugal, or inertial forces drive particle motion. Similarly, a plethora of techniques exist for the detection of cells or molecules in fluidic environments. Among these, surface-plasmon resonance, fluorescence, quantum dots (QDs), impedance spectroscopy, chromatography, nuclear magnetic resonance, and amperometric-based sensing are the most widely employed in microfluidic devices. Of general interest are several reviews and monographs on microfluidic techniques for the manipulation and detection of cancer cells/biomarkers [1, 6–11].

In this paper, we review the most recent developments in microfluidic devices for cancer cells/biomarkers manipulation and detection. Nevertheless, we have constrained our review to four methods. The first two, immunomagnetic-affinity-based capture and dielectrophoretically based capture, serve the purpose of cells/biomarkers manipulation; while the last two methods, plasmonic screening and cell-tagging based on QDs, serve the purpose of cells/biomarkers detection. For manipulation devices we systematically review the capture/removal efficiency, while for detection devices we focus on the limit of detection. However, where available, other important features of the devices (processing time, sample volume, linear range, sample purity etc.) are provided. We envisage these methods as potential candidates for the development of high-purity CTCs sorting and detection platforms. In the discussion that follows, we provide our perspective on such microfluidic devices.

2 Immunomagnetic-affinity-based capture

In cell immunoaffinity, surfaces of microchannel walls and embedded microstructures are functionalised with antibodies
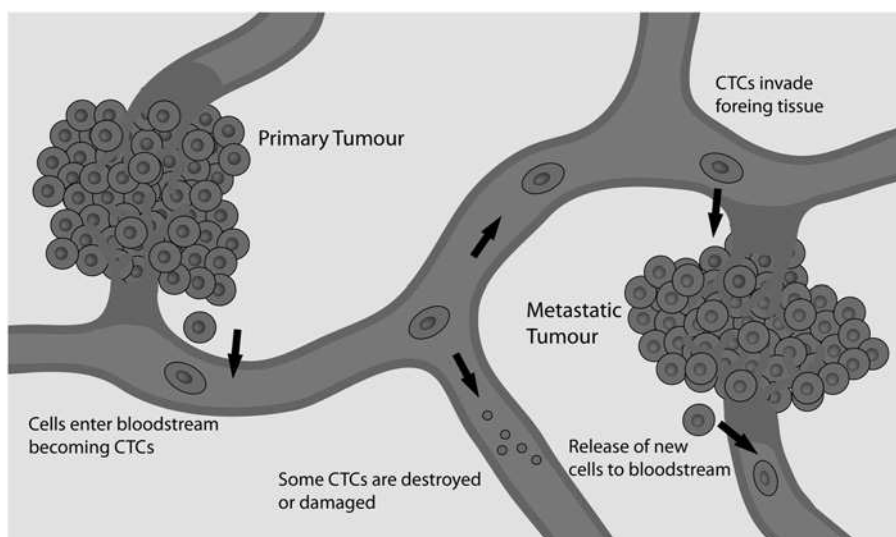
Fig. 1 *Schematic diagram of the metastasis process. First, the angiogenesis process is activated to meet the oxygen requirements of the cancerous cells in the primary tumour (left side of the diagram), leading to the formation of new vessels. Meanwhile, downregulation of cell-adhesion molecules occurs, leading to cancer cell detachment from the primary tumour, invasion of surrounding stroma and intravasation. Once in the vessels, some CTCs (elliptical cells) travel to distant organs while others are destroyed or damaged. Those that survive, may extravasate, invading foreign tissue and the few that survive the response from the innate immune system lead to the formation of a metastatic tumour (right side of the diagram). The process is repetitive. Cancerous cells that form the mestastatic tumour, may feature different traits, e.g. more malignancy, than those of the primary tumour.*

specific to an antigen expressed on the surface of a cell of interest. When the sample containing that cell is pumped into the microchannel and the cell hits the functionalised surface, a bond is formed between the antibody and the antigen, isolating the cell from the rest of the sample. Two different cell-isolation strategies (positive and negative enrichment) can be implemented. In positive enrichment, CTCs are captured at functionalised surfaces while the rest of the sample flows freely through the channel. In contrast, in negative enrichment, CTCs flow freely through the channel, while the rest of the sample is captured at functionalised surfaces [9].

Magnetophoresis is the force exerted by a non-uniform magnetic field over a superparamagnetic particle. Such force can act in two different ways. It can pull the particles to the zones of high field gradient when the magnetic susceptibility of the particle is greater than that of the suspending medium, or it can push them away from these zones when the magnetic susceptibility of the particle is smaller than that of the suspending medium [12]. Therefore, magnetic micro- and nano-particles can be functionalised with the same antibodies employed in cell immunoaffinity approaches, mixed with the sample containing the cells of interest and, due to the antigen–antibody interaction, attached to the surface of the cells. Particles act as labels, allowing to pull tagged cells toward magnetic capture zones, isolating them from the rest of the sample. The combination of magnetophoresis and cell immunoaffinity has led to the development of a new generation of microfluidic devices for early cancer detection (see Table 1).

2.1 Unobstructed microfluidic channels for CTC capture

Hoshino *et al.* [13] employed a polydimethylsiloxane (PDMS) microchannel placed above an array of magnets to capture COLO205 and SKBR3 cells _ENREF_1. Target cells were labelled employing iron(II,III) oxide (Fe_3O_4) magnetic nanoparticles conjugated to anti-epithelial-cell-adhesion-molecule (anti-EpCAM) antibodies and pulled toward the zones of highest magnetic field gradient with an efficiency (number of captured target cells/total number of target cells) of ∼90% for flow rates ≤10 ml/h. This PDMS-based cell-sorting device requires 25% less magnetic particles than CellSearch® and matches its performance. Employing a similar PDMS-based microfluidic channel, Wu *et al.* [17] developed a versatile immunomagnetic nanocarrier platform

for the capture of CTCs. In this paper, gold (Au)-shell/Fe_3O_4-core nanoparticles were employed to tag cells. In their functionalisation strategy, nanoparticles were conjugated to several antibodies including: anti-epidermal-growth-factor-receptor (anti-EGFR), anti-Ep-CAM, anti-human-EGFR-receptor-2 (anti-HER2), anti-cytokeratin (anti-CK), and anti-mucin 1 (MUC1). This strategy was evaluated versus the A431, SKBR3, COLO205, and BT20 cell lines. It was found that magnetic particles conjugated to more than one family of antibodies constitute more efficient labels than particles conjugated to a single family of antibodies (∼20% improvement in capture efficiency). Nonetheless, the device was only tested with flow rates as high as 2.5 ml/h, making it a slower alternative to other technologies Watanabe *et al.* [20] presented a pre-clinical study in which they characterise the performance of 'on-chip-sort', a novel bench-top cell-sorter, for the sub-classification of lung cancer cell lines according to their expression of CK, vimentin, and cluster of differentiation 45 (CD45). The sample analysed with the on-chip-sort system was pre-enriched using a microfluidic device similar to those described above. Magnetic beads functionalised to anti-CD45 antibodies were employed to negatively enrich A431, A549, H292, HCC827, H1975, H1755, and Hs578T cells. Pre-enriched blood samples were then analysed with on-chip-sort, achieving capture efficiencies ≥80% with the cells remaining viable after the capture.

The position, orientation, and/or alignment of the magnets also have a significant effect on CTCs capture. In [16], Huang *et al.* used spacers to set the magnet in a given position atop a PDMS-based microfluidic device and avoid CTCs agglomeration close to the inlet. The device was tested with COLO205, PC3, and SKBR3 cells, as well as with clinical samples, achieving a capture efficiency ≥90% for a flow rate of 2.5 ml/h. Additional proof of the magnet orientation effect on CTC capture is found in [14], where Forbes *et al.* proposed a PDMS-based microfluidic device featuring an angled magnet for MCF-7 cell isolation at flow rates as high as 33 ml/h. In [18], Han *et al.* used an array of angled ferromagnetic wires in a microfluidic channel to develop a reverse-transcription polymerase-chain-reaction microfluidic device. Magnetic nanoparticles were functionalised with oligo-dt primers and used to label CTCs. The device was shown to be capable of continually performing mRNA extraction, cDNA synthesis, and gene amplification from clinical samples. Moreover, Liu *et al.* [19] used soft lithography and Au deposition to produce a microfluidic channel featuring two strip-aligned electrode chips.

Table 1 Immunomagnetic-affinity-based microfluidic sorting devices

Reference	Cancer studied	Target cells/molecules	Type of microfluidic channel	Device characteristics	Capture/removal efficiency	Working solution
Hoshino et al. [13]	colon, breast	COLO205, SKBR3	unobstructed	PDMS microchannel above an array of magnets	90% for COLO205 86% for SKBR3	blood from healthy donors spiked with cancer cells
Forbes and Forry [14]	breast	MCF-7	unobstructed	PDMS microchannel with angled magnet	N/A	cancer cells suspended in Dulbecco's modified eagle medium (DMEM)
Banerjee et al. [15]	colon, liver	HCT116	unobstructed	MDNS	~80%	cancer cells suspended in human peripheral blood mononuclear cells
Huang et al. [16]	colon, prostate, breast	COLO205, PC3, SKBR3	unobstructed	PDMS microchannel with magnet and spacers	>90%	clinical samples
Wu et al. [17]	skin, breast, colon	A431, SKBR3, COLO205, BT20	unobstructed	PDMS microchannel with an array of magnets	Ranges from 93 ± 10 to 45 ± 8%	blood from healthy donors spiked with cancer cells
Han et al. [18]	breast	SKBR3	unobstructed	multichamber PDMS-based microfluidic channel above an array of ferromagnetic wires	N/A	clinical samples
Liu et al. [19]	breast	MCF-7	unobstructed	microfluidic chamber with two stripe-aligned electrode chips to generate a magnetic field	~88%	cancer cells suspended in PBS
Watanabe et al. [20]	skin, lung, breast	A431, A549, H292, Hcc827, H1975, H1755, Hs578T	unobstructed	disposable microfluidic chip to use in the on-chip-sort system	~85%	blood from healthy donors spiked with cancer cells
Horak et al. [21]	breast	MCF-7	with embedded structures	self-assembled pillars made from antibody-coated superparamagnetic microbeads	50%	cancer cells suspended in DMEM
Earhart et al. [22]	lung, breast, prostate, bladder	H1650, HCC827, MCF-7, LNCaP, PC3, T24	with embedded structures	photolithographically patterned silicon nitride membrane	~91%	clinical samples
Autebert et al. [23]	breast, prostate, lung	MCF-7, SKBR3, MDA-MB-231, PC3, A549	with embedded structures	new generation of the Ephesia system with enhanced design for high-velocity homogeneity	>90%	clinical samples
Wang et al. [24]	lung	A549	with embedded structures	PDMS microfluidic channel that integrates an array of silicon nanowires on the substrate, which enhances magnetic cell capture	~85%	clinical samples
Kang et al. [25]	breast	M6C	multi-section	PDMS microchannel with collection side chambers and an array of magnets	~90%	transgenic mouse breast cancer model
Ozkumur et al. [26]	breast, prostate	MDA-MB-231, PC3-9, SKBR3, MCF-10A	multi-section	silex microfluidic channel with four magnets in quadrupole configuration (CTC-iChip)	ranges from 95 to ~10% as a function of target cell	blood from healthy donors spiked with cancer cells
Karabacak et al. [27]	melanoma, breast, lung, prostate	WM164, MDA-MB-231, PC9 PC3, SKBR3	multi-section	CTC-iChip and its enhanced version CTC-iChip2 fabricated from SU-8 and PDMS	97%	blood from healthy donors spiked with cancer cells
Hyun et al. [28]	breast	MCF-7, SKBR3, MDA-MB-231	multi-section	two-stage microfluidic chip in which the first stage elutes WBCs and the second stage selectively isolates CTCs	>90%	blood from healthy donors spiked with cancer cells
Kirby et al. [29]	breast	MCF-7	multi-section	CD-microfluidic platform with embedded magnets	>80%	blood from healthy donors spiked with cancer cells
Mohamadi et al. [30]	prostate	VCaP	multi-section	four-zone microfluidic device that allows to separate cells according to EpCAM expression	~90%	blood from healthy donors spiked with cancer cells
Malhotra et al. [31]	oral	IL-6, IL-8, VEGF, VEGF-C	biomarker-protein	PDMS-based microfluidic device incorporating an eight-electrode array for electrochemical sensing	~90%	serum clinical samples
Bettazzi et al. [32]	lung, brain	Calu1, U87MG, T98G, H460	biomarker-protein	microfluidic device gravi-cell	N/A	cancer cells suspended in DMEM/Roswell park memorial institute medium (RPMI)
Zitka et al. [33]	prostate	sarcocine	biomarker-protein	3D printed biodegradable polymer poly-lactic acid microfluidic chip with a movable magnet	~95%	urine clinical samples
Lee et al. [34]	breast, bladder	methyladted RARβ gene	biomarker-protein	a novel methylation-specific amplification/detection device based on a microfluidic platform.	N/A	Mspl solution Hpall solution
Otieno et al. [35]	leukaemia	IL-6, IL-8	biomarker-protein	PDMS capture chamber with holes to integrate an amperometric measurement platform	N/A	proteins suspended in PBS
Lin and Peng [36]	bladder	APOA1 antigen	biomarker-protein	PDMS-based five-layer microfluidic channel that integrates EIS with pneumatic actuation	N/A	urine clinical samples

In this paper, pulsatile alternating current (AC) signals were applied to two parallel sets of straight conducting wires to generate a magnetic field. The performance of the device was characterised using magnetic beads conjugated to anti-EpCAM antibodies and MCF-7 cancer cells, achieving a capture efficiency of ~88%, and with the cells remaining viable after capture.

A different approach was introduced in [15], where Banerjee *et al.* presented a magneto-dendritic-nanosystem (MDNS) for the targeting, isolation, and detection of HCT116 and HepG2 cells in blood samples. In this paper, the MDNS platform was synthesised by functionalising Fe_3O_4 magnetic nanoparticles with fourth generation polyamidoamine (PAMAM) dendrimers through glutathione. Cyanine 5 NHS and transferrin receptors expressed on the membranes of CTCs can simultaneously attach to PAMAM dendrimers through covalent bonding. Employing a fluidic chamber, an external magnet, and high-resolution imaging, it was demonstrated that the MDNS achieved a CTC capture yield of ~80% in a 5 min time frame.

It is evident that many parameters play a significant role in the capture of cancer cells in immunomagnetic-affinity-based unobstructed microfluidic devices. Flow rate, for example, dictates the amount of time required to analyse a given volume of sample. Some of the devices reviewed above feature high capture efficiencies (~90%), but can only process samples at low flow rates (e.g. 2.5 ml/h), hindering their applicability in clinical trials. However, the optimisation of channel geometry and positioning of the permanent magnets have resulted in increased flow rates (e.g. 33 ml/h). Unfortunately, post-capture cell viability is a feature shared by only a small number of devices, making it unlikely for the rest to become a clinically feasible technology for the manipulation of cancer cells.

2.2 Microfluidic channels with embedded structures for CTC capture

In [21], Horák *et al.* fabricated magnetic poly(glycidyl-methacrylate) microbeads conjugated to anti-EpCAM antibodies, and used them to build self-assembled arrays within a microfluidic chamber to capture MCF-7 cells. With this it was possible to attain flow rates of 2 ml/h. This trapping method is known as the Ephesia system. Then, in [23], Autebert *et al.* presented a new generation of the Ephesia system that allows for high capture yield (≥90%) and purity (~99%) with the same 2 ml/h flow rate with the cells remaining viable after capture. In this improved version, a filtering zone was integrated at the entrance of the chip to avoid channel clogging due to dust or debris. The Ephesia system was employed to capture MCF-7, SKBR3, MDA-MB-231, PC3, and A549 cells and to screen clinical samples.

Another efficient device was presented in [22], where Earhart *et al.* utilised low-pressure chemical-vapour-deposition, photolithography, and plasma and reactive-ion etching to create pore arrays on a silicon wafer. Thereafter, a thick permalloy film was deposited on the wafer surface employing high-vacuum RF-sputtering. On application of an external magnetic field, extremely high field gradients developed at the pore edges. This translates into very efficient cell capture capabilities (>90%). Moreover, as the silicon chip is a square with an area of 49 mm², high throughput is achieved due to the very high density of fabricated pores (~200 pores/mm²). The device was tested with H1650, HCC827, MCF-7, LNCaP, PC3, or T24 cells, which remained viable after capture. Magnetic beads were conjugated to anti-EpCAM antibodies to label the cells.

Silicon nanowires have also been employed as mechanical traps to improve capture yield. In [24], wet etching was employed by Wang *et al.* to fabricate an array of silicon nanowires embedded in a PDMS microfluidic channel for CTCs capture. The channel was placed above a permanent magnet and tumour cells were captured using anti-EpCAM conjugated magnetic up-conversion nanoparticles. The capture efficiency of the device was compared with that of a planar device and was found to be significantly higher. Also, cells remained viable after capture. About 21 clinical samples (staged

with TNM classifications) were sorted and analysed with this device. Results obtained with the silicon-nanowire-based microfluidic chip accurately classified the 21 samples according to the stage of the disease.

In comparison with immunomagnetic-affinity-based unobstructed microfluidic devices, the devices presented in this section were shown to require more time to process a sample of a given volume. This is due to the very low flow rates exhibited by these devices (~2 ml/h). However, they also feature attractive traits that may turn them into clinically feasible techniques for the manipulation of cancer cells. For example, they not only feature high capture efficiencies, but also high capture purities (~99%) with cancer cells remaining viable after capture for most of the devices reviewed herewith.

2.3 Multi-section microfluidic devices for CTC capture

As the flow-velocity within a microfluidic channel is influenced by the dimensions of the channel, and knowing that CTCs have different levels of EpCAM antigen-expression on their surface, Mohamadi *et al.* [30] developed a four-zone microfluidic device that exerts a drag force with different magnitude in each zone. In this paper, magnetic beads conjugated to anti-EpCAM antibodies were employed to label a population of VCaP and U937 cells. Owing to the differences in antigen-expression, each cell was labelled with a different number of magnetic nanoparticles. A capture efficiency of 90% with a sub-category purity >95% was achieved with this design. Moreover, cells were shown to remain viable after the sorting process. This device was tested with flow rates as high as 40 ml/h.

Aiming to develop a high capture-purity device, Kang *et al.* [25] introduced a novel PDMS-based microfluidic channel featuring a filtration zone, a couple of fluidic channels, and several side chambers for cell capture. Magnetic beads were conjugated to anti-EpCAM antibodies and M6C cells were employed to assess the performance of the microfluidic chip. A capture efficiency of ~90% with a purity of ~98% was achieved with this device. For this, a rather low flow rate of 1.2 ml/h was employed. Most of the cells captured with this device remained viable after capture. An innovative two-section microfluidic chip was presented by Hyun *et al.* in [28], where white blood cells (WBCs) were eluted in the first section employing magnetically activated-cell-sorting, whereas CTCs were captured through cell immunoaffinity in the second one. MCF-7, SKBR3, and MDA-MB-231 cancer cells were used to characterise the performance of the device. While the capture efficiency of the device is ≥90%, the purity of the captured cell population exhibited a significant variability as a function of cell concentration ratios (e.g. [MCF-7]/[SKBR3]). Flow rates as high as 24 ml/h were employed to test the sorting capabilities of the device. More sophisticated multi-section devices have also been developed. The so-called 'CTC-iChip' introduced by Ozkumur *et al.* in [26] was fabricated through deep-reactive-ion etching and soft lithography on silicon wafers. It integrated three zones of operation. In the first zone, an array of posts directed red blood cells (RBCs), platelets, and other blood components to one outlet, whereas WBCs and labelled CTCs were directed toward the second zone. Therein, a serpentine-like microfluidic channel focused WBCs and CTCs into a single streamline. Finally, the magnetophoresis zone, redirected the labelled CTCs to one outlet and the WBCs to another outlet. The chip was tested with MDA-MB-231, PC3-9, SKBR3, or MCF-10A cells and magnetic beads conjugated to anti-EpCAM antibodies. Capture efficiencies as high as 95% were obtained with capture purities >90% at a flow rate of 8 ml/h. Enhanced CTC-iChip devices were presented in [27], where capture efficiencies of 97% were reported.

A completely different approach was presented in [29], where immunomagnetic manipulation of CTCs was carried out exploiting CD-microfluidic technology. Kirby *et al.* developed a PDMS-based CD-cartridge with embedded magnets and independent channels to isolate, in parallel, CTCs from several blood samples. MCF-7

cancer cells and paramagnetic nanoparticles conjugated to anti-EpCAM antibodies were employed to assess the performance of the CD-cartridge. The disk containing the labelled cells was rotated with a frequency of 17 Hz during 10 min, attaining a capture efficiency of ∼88% and not affecting the viability of the cells.

In comparison with devices reviewed in the two previous sections, multi-section microfluidic devices offer the possibility of sorting cells as a function of a particular feature (e.g. size) within a single device. Flow rates used to test these devices range from 1.2 to 40 ml/h, making them attractive alternatives to conventional cell-sorting methods. Nonetheless, devices reviewed herein have not yet been tested with blood samples obtained from cancer patients. Therefore, they do not constitute a clinically relevant technology yet.

2.4 Microfluidic devices for the detection of cancer biomarkers

In [31], Malhotra et al. introduced a nanostructured microfluidic array for the ultra-sensitive detection of cancer biomarkers. In this paper, through the conjugation of magnetic beads to anti-IL-6, anti-IL-8, anti-vascular endothelial growth factor (VEGF), and anti-VEGF-C antibodies, the authors performed multiplexed biomarker-protein detection in clinical samples from oral cancer patients. A two-section PDMS microfluidic device was utilised for the magnetophoretic manipulation and subsequent electrochemical detection of labelled proteins, achieving a capture efficiency of ∼90% with a capture purity of ∼98%. This microfluidic device achieved femtomolar detection limits for the four target biomarker-proteins. An extension of this paper was presented in [35], where Otieno et al. integrated an online protein capture chamber, fabricated from PDMS and PMMA, into the modular microfluidic system. Additionally, magnetic beads were coated with ∼40,000 antibodies and ∼300,000 enzyme labels for protein capture. The device required 30 min to complete the analysis, in contrast to the 50 min required by the off-line scheme [31].

Strategies based in the use of DNA and RNA have also been proposed for the early detection of cancer. In [32], Bettazzi et al. presented an electrochemical (immunomagnetically assisted) method for the detection microRNA (miRNA)-222. First, miRNAs are biotinylated while streptavidin (SA)-coated paramagnetic beads are functionalised with biotinylated DNA capture-probes. Thereafter, miRNAs and paramagnetic beads are hybridised, incubated with SA alkaline phosphatase, and exposed to α-naphthyl-phosphate. Next, particles are magnetically captured at the surface of disposable screen-printed electrodes, which are also used for the electrochemical monitoring of the enzymatic product (α-naphthol) through differential pulse voltammetry. This device was tested employing U87MG, T98G, Calu1, and H460 cells, achieving a limit of detection of ∼7 pmol/l. In the same direction, Lin and Peng [36] introduced a bead-based immunoassay combined with DNA strand labelling for the detection of cancer biomarkers. A five-layer PDMS microfluidic assembly with an integrated electrochemical impedance spectroscopy (EIS) sensor was employed in this paper. Urine samples from bladder cancer patients were used to assess the performance of the proposed device. Briefly, magnetic beads were conjugated to HDL110 monoclonal antibodies. Then, antigen APOA1 bound to the HDL110 antibodies. A second antibody, HDL44, was introduced to the fluidic channel and it bound to the APOA1 protein. Afterwards, DNA–SA complexes were added and bound to HDL44 antibodies. Finally, an external magnet was employed to produce a magnetic field within the channel and capture the modified magnetic beads at the EIS sensor. The total time required by the platform to perform the immunoassay test was 1 h. The performance of the microfluidic detection device was compared with that of a traditional enzyme-linked immunosorbent assay test and was found be within an error margin of 20%.

One important concern in the field of microfluidic developments for DNA-based cancer detection is the time required to analyse the sample. In this direction, Lee et al. [34] introduced a microfluidic platform for DNA methylation-specific amplification/detection and tested it to detect the presence of MCF-7 and T24 cells in a fluidic sample. The platform is composed of an on-chip digestion device and a methylation-specific isothermal solid-phase amplification/ detection (ISAD) device. Human genomic-DNA extraction was carried out after MCF-7 and T24 culture in the presence of proteinase K. DNA was then modified employing a bisulphite conversion kit and mixed with magnetic beads conjugated to human MBD protein 2. DNA could then be isolated from the sample on application of an external magnetic field. Afterwards, captured DNA was recovered from the beads, eluted, mixed with recombinase polymerase amplification solution, and sent to the ISAD device for the simultaneous amplification and detection of the retinoic acid receptor beta (RARβ) gene. Results demonstrated that this microfluidic platform requires 65 min to detect methylated *RARβ*, which represents a reduction of 50–80% in comparison with other off-chip and on-chip methylation analysis methods.

With the objective to screen urine samples for the detection of prostate cancer, Zitka et al. [33] developed a three-dimensional (3D)-printed biodegradable polymer poly-lactic acid microfluidic chip, which features a movable permanent magnet for the capture of *N-methylglycine*. To detect the presence of sarcosine, silica particles were first modified to feature an iron(III) oxide surface coverage, obtaining paramagnetic properties. The beads were then introduced in the channel and washed with binding buffer, obtaining SO_3^- functional groups. Then, sarcosine amino acids were bound to the paramagnetic beads and magnetically captured. The captured particles were then effectively resuspended and recovered at the channel outlet, making this device an attractive alternative to the usual prostate cancer detection tests such as examination per rectum and transrectal sonography with a biopsy of prostate tissue.

The devices reviewed herein feature detection limits as low as a few pmol/l, which lies within the clinically relevant detection margin for most biomarkers (as will be discussed in Section 4). Nevertheless, as these devices require the integration of different technologies to accomplish manipulation and detection of the biomarkers, their fabrication process is generally cumbersome and more expensive than the ones employed to develop the devices reviewed in the previous three sections.

3 Dielectrophoresis (DEP)-based capture

In microfluidics, electrokinetic forces are used to manipulate particles and fluids due to electrostatic interactions. Whenever an electric field is in the presence of a heterogeneous system (i.e. ions in water), particles in the system undergo forces that allow their manipulation according to the properties of the particles and the system [37]. Among such forces, DEP is widely used to manipulate neutral particles (such as cells). Briefly, DEP relies on induced polarisation effects on the cell when it is in the presence of non-uniform electric fields. The dielectrophoretic force exerted on a cell is related to its size, dielectric properties, and the gradient of the electric field square generated by the microdevice [38]. This force can either be positive (pDEP), attracting particles to the zones of highest field gradient when particles are more polarisable than the suspending medium, or negative (nDEP), repelling them from such zones when the medium is more polarisable than the particles. When working with AC fields, it is possible to find a frequency at which no DEP effect can be observed. This frequency is known as the cross-over frequency and gives important information about the dielectric properties of the cell under study [39]. The reader is referred to [40] for a detailed description of DEP theory and a thorough discussion on DEP-based technology and applications.

To produce non-uniform electric fields, microdevices are traditionally equipped with electrode arrays, i.e. electrode-based DEP (eDEP), fabricated at the bottom of microchannels where AC electric potentials are applied to produce gradients of the electric field square [41]. In contrast, in other designs, insulator structures are fabricated between electrodes to create regions of high field gradient, technique known as insulator-based DEP (iDEP) [42].

Table 2 DEP-based microfluidic sorting devices

Reference	Cancer studied	Cells studied	DEP device	Device characteristics	Capture/removal efficiency	Working solution
Gascoyne et al. [43]	leukaemia	mouse erythroleukemia	eDEP	shifted interdigitated castellated electrodes fabricated in Au	N/A	320 mM sucrose solution containing 2 mg/ml of dextrose
Moon et al. [44]	breast	MCF-7	eDEP	hybrid of MOFF and DEP with interdigitated Au electrodes slanted at −15° and 15°	75.81% of malignant cells	isotonic 8.5% sucrose and 0.3% dextrose with PBS and 1% bovine serum albumin (BSA)
Mulhall et al. [45]	oral	H-357, H-157	eDEP	microwell electrode system	N/A	17 mM glucose and 263 mM sucrose in deionised water with PBS
Gupta et al. [46]	ovarian, breast	SKOV-3, MDA-MB-231	eDEP	copper and Au interdigitated electrodes	75.4% for SKOV-3 and 71.2% for MDA-MB-231	RPMI cell culture growth medium with BSA, pluronic F-68, and antioxidants
Wu et al. [47]	colon	HT-29	eDEP	interdigitated ITO electrodes.	N/A	8.5% sucrose and 0.3% glucose buffer.
Fabbri et al. [48]	lung, colon	A-549, mCRC	eDEP	square-electrode array	10–80% depending on the initial malignant cell concentration	peripheral blood
Huang et al. [49, 50]	prostate	LNCaP	eDEP	Hele-Shaw flow cell with interdigitated Au electrodes functionalised with the monoclonal antibody (J591)	average ratio of 2.94 of immunocaptured cell densities with DEP to without DEP	isotonic 9.5% sucrose and 0.3% dextrose in deionised water and PBS
Huang et al. [51]	pancreatic	Capan-1, PANC-1, and BxPC-3	eDEP	Hele-Shaw flow cell with interdigitated Au electrodes functionalised with the monoclonal antibody (anti-EpCAM)	average ratio of immunocaptured cell densities with DEP to without DEP: 2.58 for Capan-1, 12.72 for PANC-1, and 15.21 for BxPC-3	isotonic 9.5% sucrose and 0.3% dextrose in deionised water and PBS
Bhattacharya et al. [52]	breast	MCF-7	iDEP	elliptic and teardrop-shaped insulators at the perpendicular crossing of two microchannels	N/A	10–30 mM 4-(2-hydroxyethyl)-1-piperazineethanesulfonic acid (HEPES) with 70–140 mM glycerol
Bhattacharya et al. [53]	breast	MCF-7, MDA-MB-231	iDEP	teardrop-shaped insulators at the perpendicular crossing of two microchannels	N/A	30 mM HEPES with 120 mM trehalose and 1 mM F-108
Smith et al. [54]	pancreatic	Capan-1, PANC-1, BxPC-3	iDEP	circular insulating posts in offsetting rows	N/A	N/A
Henslee et al. [55]	breast	MCF-7, MDA-MB-231	cDEP	straight sample channel with circular insulators	total capture determined at 90% or higher of cells captured	DEP buffer
Sano et al. [56]	leukaemia	THP-1	cDEP	straight channel with saw-tooth structures	N/A	solution with 8.5% sucrose, 0.3% glucose, and 0.725% RPMI
Sano et al. [57]	leukaemia, breast	THP-1, MDA-MB-231	cDEP	straight channel with saw-tooth structures	N/A	solution with 8.5% sucrose, 0.3% glucose, and 0.725% RPMI
Salmanzadeh et al. [58]	prostate	PC3	cDEP	high-throughput channel with multiple circular insulators	total capture determined at 100% of cells captured	solution with 8.5% sucrose, 0.3% glucose, and 0.725% RPMI
Salmanzadeh et al. [59]	ovarian	MOSE	cDEP	high-throughput channel with multiple circular insulators	total capture determined at 100% of cells captured	solution with 8.5% sucrose, 0.3% glucose, and 0.725% RPMI
Sano et al. [60]	breast	MDA-MB-231	cDEP	multilayer device with a straight sample channel with saw-tooth structures	N/A	N/A
Salmanzadeh et al. [61]	ovarian	MOSE	cDEP	straight channel with saw-tooth structures	N/A	solution with 8.5% sucrose, 0.3% glucose, and 0.725% RPMI
Demircan et al. [62]	leukaemia	K562	cDEP	3D-electrode array surrounding a channel with C-shaped barriers	N/A	isotonic 8.5% sucrose with 0.3% dextrose

Another alternative is available in which microfluidic channels are filled with a high-conductive liquid and used as electrodes. Such liquid electrodes are separated from the sample channel by thin insulating barriers that exhibit a capacitive behaviour. When electric potentials are applied across these side channels, electric gradients are created in the sample channel inducing DEP. This technique is known as contactless-DEP (cDEP).

Below, the work reported during the past years for the application of DEP to manipulate cancer cells is divided into four types of devices described (eDEP, iDEP, and cDEP), and a brief summary is given in Table 2. Most of the microfluidic devices presented herewith do not constitute a clinically feasible alternative solution to cells sorting yet. Nevertheless, they are included in this review due to their potential to exploit morphological and dielectric differences between cancerous and non-cancerous cells for specific manipulation. For the devices to become a feasible alternative

solution to cell sorting, the throughput of the devices must increase considerably. iDEP and cDEP designs are on track in this aim, but 3D-electrode-based systems also have a great potential for high-throughput cell manipulation. Some works in the area include the use of electroplated electrodes [63], doped-silicon (Xing et al.) [64] or PDMS [65], carbon-electrodes (carbon-MEMS) [66], or electroconductive-polymers [67], among others; which yet have to be tested with cancer cell lines to evaluate their effectiveness in the area. Though these structures can be difficult and expensive to manufacture in some cases, advances in microfabrication make these procedures more feasible for a near future.

3.1 Electrode-based DEP

The first research work on the dielectrophoretic manipulation of cancerous cells was reported by Gascoyne et al. in 1992 [43]. In this

paper, the authors reported separation of erythroleukaemia cells from normal murine erythrocytes, which exhibited pDEP and nDEP, respectively, in a device with shifted interdigitated castellated electrodes fabricated in Au. Other works that helped pioneer this research field include those of Becker *et al.* [68, 69], where breast cancer cells and leukaemia cells were dielectrophoretically manipulated. More recently, Moon *et al.* [44] proposed a hybrid device which combined a section for multi-orifice flow fractionation (MOFF) and a section for DEP that comprised an array of interdigitated Au electrodes slanted at −15° and 15°. In the MOFF section, the device had 80 contraction and expansion chambers to sort particles by size in correlation with the Reynolds number. Afterwards, the targeted MCF-7 cells were further focused at the centre of the device with pDEP and separated from RBCs and WBCs. This novel device takes advantage of two different separation techniques in combination within a single microfluidic device to increase cell manipulation efficiency. To evaluate the differences in the electrical properties of normal, pre-cancerous, and cancerous oral keratinocytes, Mulhall *et al.* [45] developed a DEP-microwell electrode system to calculate the cytoplasm and membrane capacitance by finding the cross-over frequency of the cells. A similar approach was proposed by Wu *et. al* in [47], where the authors used interdigitated ITO electrodes to determine the dielectric properties of the cytoplasm and membrane for HT-29 cells as a function of medium conductivity. The results obtained were used to selectively capture either HT-29 cells or RBCs in a mixture, by varying the stimulation voltage.

Commercially available devices that use DEP to detect and collect CTCs from blood samples have also been presented. Gupta *et al.* [46] introduced their system ApoStream^{TM} that uses a microchannel with an Au and copper interdigitated electrode array to continuously sort cancer cells from a sample, allowing the analysis of large blood volumes. While peripheral blood mononuclear cells (PBMCs) experience nDEP and are levitated away from the bottom of the channel, SKOV-3 or MDA-MB-231 cancer cells are held close to the electrodes at the bottom and get collected for further analysis. Another device, named DEPArray^{TM}, introduced by Fabbri *et al.* [48], uses an array of ∼ 30,000 electrodes, where each one can be individually controlled. This allows for a multiplicity of DEP cages per cartridge, where labelled A549 and metastatic colorectal cancer (mCRC) cells are captured and then analysed through high-quality image-based selection for their identification and isolation. Despite DEPArray^{TM} relies on DEP to isolate cells from a sample, their redirection for collection is decided on fluorescence and morphological characteristics of the cells. Therefore, while DEP-based systems present the advantage of labelless identification and separation of samples, this device requires fluorochrome usage for identification of a cell as cancerous.

In 2013 and 2014, Huang *et al.* [49, 50] published on the characterisation and application of a hybrid Hele-Shaw flow cell with interdigitated Au electrodes functionalised with a monoclonal antibody specific to the prostate-specific membrane antigen, J591, thus combining microfluidic immunocapture and DEP. The dielectrophoretic force was demonstrated to have an influence on the performance of the shear-dependent capture of the device by promoting or avoiding cell interactions with the capture surfaces. Later, with a similar device, Huang *et al.* [51] reported the performance of the Capan-1, PANC-1, and BxPC-3 cancer cells immunocapture when in the presence of PBMCs. As before, through the careful selection of an electric field for which the cancer cells exhibit strong pDEP while the PBMCs experience nDEP, the positive interactions were enhanced. These works are examples of the complementation of techniques in order to improve the performance of a device. In this case, the capture efficiency for other desired cells will depend on the correct selection of the monoclonal antibody and the capacity of their immobilisation into the pDEP designed sites of the channel.

3.2 Insulator-based DEP

There are fewer reports on the use of iDEP devices than for eDEP; nevertheless, successful applications of the technique

have been published. In 2011, Bhattacharya *et al.* [52] presented a device with a main channel and a perpendicular side channel, with insulating structures embedded at the centre of the crossing to produce the non-uniform electric fields. With the device having two teardrop-shaped insulators, the authors were able to capture a single MCF-7 cell through nDEP. Later, the device was used to selectively isolate a single MCF-7 cell when in mixture with PBMCs, and an MDA-MB-231 cell in a 1:1 ratio with PBMCs [53]. In these studies, the authors focused on single cell capture and manipulation, in the aim of evaluating the response of a cell to different stimulus, allowing its downstream analysis.

A second report for the application of an iDEP device was presented by Smith *et al.* [54]. Their device consisted of a microchannel with circular insulating posts in slightly offsetting rows, and two electrodes that generated the electric field perpendicular to the flow and directly across the section of the insulators. The study was focused on producing pDEP to attract cells to the functionalised posts, enhancing their interaction with monoclonal antibodies. In this paper, BxPC-3, Capan-1, and PANC-1 cells were used to model pancreatic CTCs, whereas PBMCs to model contaminating leukocytes. The collision rate of target cells against functionalised surfaces was found to be favoured through pDEP, which would increase the immunocapture response of the device. Predictions obtained from computational modelling show that this device has great potential to increase the interactions of pancreatic cancer cells with their antibodies. Nevertheless, the study is very specific to those cell lines. To analyse the performance of the device with other cells, a similar study can be conducted by knowing their capture parameters previously.

3.3 Contactless DEP

A very promising class of dielectrophoretic devices, especially for manipulating mammalian cells, is cDEP-based devices. This is because the method avoids contact of the sample with the electrodes, making the designs very attractive for handling biological samples. Henslee *et al.* [55] employed a cDEP-based device (consisting on a straight channel with embedded insulating posts, where lateral liquid electrodes were used to generate the non-uniform electric field) to evaluate the difference in the dielectrophoretic response of breast cancer cells according to the progression of the disease. In this paper, a heterogeneous sample of MCF-7, MCF-10A, and MDA-MB-231 cells was studied, and it was found that the MDA-MB-231 cells can be isolated from the mixture.

A larger device was introduced by Salmanzadeh *et al.* [59]. The design included arrays of insulating circular posts to immobilise targeted cells by means of pDEP on a high-throughput microchannel. The device was used to evaluate the intrinsic properties of ovarian cancer cells (mouse ovarian surface epithelium (MOSE)) in their different stages of the disease (early, early/intermediate, intermediate, and late cancer), by finding and comparing their capture voltage. The authors reported that the voltage required to immobilise the cells increases as the cancer progresses in its stage, which could be a result of membrane proteins expression and membrane ruffling as the cells differentiate into more aggressive phenotypes. The device was also used by Salmanzadeh *et al.* [58] to isolate prostate tumour-initiating cells (TICs) when in a mix with non-TICs. An AC-electric potential was used to isolate TICs from non-sorted PC3 cells. The immobilised population was cultured after collection and was observed to present spheroids, characteristic for TICs, as opposite to non-captured cells. The device was able to differentiate subtle variations in membrane capacitances of the cells, which represent a great potential for many other applications. Unfortunately, owing to the insulating barriers impedance, the device cannot operate at frequencies below 100 kHz.

cDEP designs that were able to operate at low frequencies, where cells present significant differences in their dielectrophoretic response (between 10 and 100 kHz), were introduced by Sano

Table 3 SPR-based microfluidic sensing devices

Reference	Cancer studied	Targeted biomarker	SPR modality	Clinically significant level	Limit of detection	Linear range	Solution
Choi and Chae [72]	thyroid	Tg	angular	N/A	1 pg/ml	1 pg/ml–1 μg/ml	PBS
Chang et al. [73]	breast	CA15-3	angular	30 U/ml	0.025 U/ml	1–40 U/ml	PBS
Chen et al. [74]	breast	VEGF	angular-RCA	N/A	100 pg/ml	100 pg/ml–1 μg/ml	TBS
Jang et al. [75]	lung	IGFBP-7	angular	N/A	10 ng/ml	10–300 ng/ml	PBS
Ladd et al. [76]	colon, ovarian	CEA	wavelength	1 μg/ml	N/A	N/A	serum
Fang et al. [77]	gastric	MG7-Ag	wavelength	N/A	N/A	N/A	serum
Springer et al. [78]	trophoblastic	hCG	wavelength	~μg/ml	10 ng/ml	N/A	50% blood plasma
Law et al. [79]	N/A	TNF-alpha	phase	N/A	0.5 ng/ml	N/A	PBS
Ladd et al. [80]	breast, colon, liver	ALCAM	SPRi	10–100 ng/ml	6 ng/ml	N/A	PBS
	breast, colon	TAGLN-2		10–100 ng/ml	3 ng/ml		PBS
Piliarik et al. [81]	trophoblastic	hCG	SPRi	~μg/ml	100 ng/ml	N/A	10% blood plasma
	breast	ALCAM		~μg/ml	45 ng/ml		10% blood plasma
Shabani and Tabrizian [82]	bladder	Fas	SPRi-QD	N/A	25 pg/ml	N/A	PBS
	angiogenesis	Ang-2					
	ovarian	MMP-9					
	breast	HER-2		15 ng/ml			
Jang et al. [83]	prostate	PSA	sSPR-FO	4.0 ng/ml	4 ng/ml	N/A	PBS
Li et al. [84]	colon, ovarian	CEA	sSPR	1 μg/ml	1.0 ng/ml	1–60 ng/ml	serum
Acimovic et al. [85]	liver	AFP	LSPR	700 ng/ml	500 pg/ml	5–1000 ng/ml	50% human serum
	prostate	PSA		4.0 ng/ml	1 ng/ml	10–100 ng/ml	50% human serum
Geng et al. [86]	liver	AFP	LSPR	700 ng/ml	25 ng/ml	N/A	PBS
Sanders et al. [87]	prostate	f-PSA	LSPR-FO	0.4 ng/ml	100 fg/ml	100 fg/ml–5 ng/ml	PBS
Hu et al. [88]	N/A	trace oligonucleotides	LSPR	N/A	3 nM	N/A	N/A

et al. [56]. The authors compared the performance of different designs for low-frequency applications, which consisted on channels with saw-tooth features to produce the non-uniform electric fields. A leukaemia cell line (THP-1) was successfully manipulated at low frequencies due to pDEP while RBCs remained unaffected. Later, one of the devices was used to investigate the dielectric properties of MDA-MB-231, THP-1, PC1, and RBCs, obtained with the cross-over frequency, as the cells were unaffected by DEP as opposite to being attracted to the top of the channel by pDEP or rejected from this area and shown closer to the bottom of the device by nDEP [57]. Salmanzadeh et al. [61] also reported the use of a low-frequency cDEP device to investigate the electric properties of ovarian cancer cells as they progress into more aggressive phenotypes.

There exist other reports on cDEP devices that are successful in manipulating cancer cells, but their fabrication is more complicated than the simple photolithographic procedures used to produce the described designs. Sano et al. [60] published the use of a multilayer cDEP device that produced similar results to previous designs, but increased the sample throughput significantly. With the device, the authors demonstrated capture of MDA-MB-231 cells at a flow rate of 1.0 ml/h. Demircan et al. [62] reported recently a contactless device with 3D-metal electrodes at the sides of a channel to produce non-uniform electric fields and produce DEP. The high-throughput sample channel had C-shaped obstacles to provide hydrodynamic focusing of the cells to the dielectrophoretic traps close to the electrode array due to pDEP. With the device, the authors reported the selective capture of leukaemia cancer cells resistant to imatinib (K562/IMA), while sensitive cells (K562) are unaffected by DEP.

4 Surface-plasmon-resonance (SPR) biosensing

SPR is currently the most common direct transduction method for transforming the biochemical response caused by analyte binding into a measurable output signal. The use of SPR sensors in biomolecular interaction analysis incorporates the convenience of label-free real-time detection with a high sensitivity and low-noise signal transduction performance. Accordingly, when integrated on microfluidic chips, SPR sensors provide a promising platform

for high-throughput, sensitive, and automatic point-of-care diagnostics [70].

The detection principle of SPR relies on the resonant oscillation of free electrons on the surface of a metal adjacent to a dielectric medium. This charge density wave is excited through illumination, with a photon–electron coupling strength highly sensitive to the optical and geometrical characteristics of the system; i.e. the conditions at which SPR takes place are very specific to the interface for a fixed incidence angle, photon wavelength, and light polarisation, as described in [71]. In this manner, when a biomolecular binding occurs at the metal, the dielectric properties of the interface change, approximately within 200 nm [72], according to the concentration of the bound analyte, and thus the resonance conditions for the electrons in the interface shift. This shift can be then resolved and measured using a photodetector.

In this section, the capabilities of different SPR sensors are discussed in terms of its achieved limit of detection and linear response range for a targeted biomarker in comparison with the clinically significant level of the associated cancer type, as summarised in Table 3.

4.1 SPR with angular interrogation

In this modality, monochromatic light is used to excite surface plasmons and the reflected light is monitored as a function of the incidence angle. Chang et al. [73] presented an SPR sensing platform with angular interrogation that implemented protein adsorption for the detection of thyroglobulin (Tg) in phosphate buffered saline (PBS) using Au/zinc oxide (ZnO) nanocomposite films. Au/ZnO layers allowed a detection limit four times lower than conventional Au/chromium (Cr) adhesion layers. Such improvement are due to Cr problems involving metal interdiffusion and low optical transmission to the Au surface. The sensor was applied to detect carbohydrate antigen 15.3 (CA15-3) in PBS with a concentration of 0.025 U/ml and a linear range of 1–40 U/ml.

Aiming to improve the limit of detection attained with this SPR modality, Chen et al. [74] implemented a rolling circle amplification (RCA) process to amplify the SPR signal. With this, VEGF was detected in Tris-buffered saline (TBS) at a

concentration of 100 pg/ml with a linear range from 100 pg/ml to 1 µg/ml. An alternative was introduced by Jang *et al.* [75] who demonstrated an SPR biosensor for the detection of insulin-like growth factor binding protein 7 (IGFBP-7), featuring a limit of detection of 10 ng/ml in PBS and a linear range of 10–300 ng/ml. For this, the authors employed a mixed self-assembled monolayer (SAM) in conjunction with a specific receptor on an Au thin film.

The devices presented in this section can also be extended to detect a wide range of targets. For example, MCF-7 cancer cells in clinical applications can be detected through the careful selection of recognition aptamers. In addition, these devices offer the advantage of real-time viewing. Therefore, SPR with angular interrogation may contribute to early tumour diagnosis and therapy in the future.

4.2 SPR with wavelength interrogation

In this modality, polychromatic light at a fixed angle is used to excite surface plasmons and the reflected light is monitored as a function of the wavelength.

An SPR sensor based on wavelength interrogation and temperature stabilisation for differentiating carcinoembryonic antigen (CEA) autoantibodies levels in serum samples was demonstrated by Ladd *et al.* in [76]. In this paper, authors were able to show that serum samples with overexpressed CEA autoantibody were distinguishable from healthy samples using a criterion based on direct detection. Later, Fang *et al.* [77] established a similar SPR sensor for the detection of gastric carcinoma-associated antigen (MG7-Ag) in human serum, with less laborious sample preparation. Detection of human chorionic gonadotropin (hCG) in 50% blood plasma was also achieved with a limit of detection of 10 ng/ml by a comparable SPR sensor and a dispersionless microfluidic system developed by Springer *et al.* [78]. This microfluidic system allows switching between two samples without dispersion of the liquid and intermixing before the sample reaches the sensing area. These works demonstrate that SPR with wavelength interrogation has potential use in rapid, real-time detection and identification of cancer biomarkers.

4.3 SPR with phase interrogation

Phase interrogation is the less common modality in SPR. It uses monochromatic light at a fixed angle to excite surface plasmons and examines the phase shift of the reflected light. Detection of tumour necrosis factor alpha (TNF-alpha) at a concentration of 0.5 ng/ml in PBS was reported by Law *et al.* [79] using an SPR with phase interrogation. The use of a highly specific sensing film and wavelength-matched Au nanotags were fundamental to the development of this sensor. The achieved detection sensitivity opens up the possibility to monitor small variation of TNF-alpha, to understand the cancer biology, and to investigate the progress of any therapeutic drug treatment. This paper demonstrated a very significant sensitivity enhancement in comparison with previous developments reported in the literature. Such improvements are due to the plasmonic field extension generated through the Au nanotags.

4.4 SPR imaging

As it is insufficient to detect only a single biomarker for accurately diagnosing a cancer stage or disease status [81, 82, 89], SPR technology has evolved to increase the number of sensing channels using imaging capabilities. This label-free modality, known as SPR imaging (SPRi), allows for the simultaneous screening of whole panels of cancer biomarkers in an array format with multiple active sites.

SPRi is based on the same principle as SPR, apart from the photodetector, which is replaced by a CCD camera so that a large number of different binding events can be spatially resolved in parallel. Employing a sensor that combined SPRi with polarisation contrast and a spatially patterned multilayer SPR structure, Ladd *et al.* obtained high-contrast SPR images suitable for automated computer analysis, minimum cross-talk between neighbouring sensing channels, and inherent compensation for light level fluctuations [80]. Detection of activated leukocyte cell-adhesion molecule/CD 166 (ALCAM) and transgelin 2 (TAGLN-2) was validated in that study. Limits of detection for ALCAM and TAGLN-2 were established at 6 and 3 ng/ml, respectively, in PBS. Similarly, Piliarik *et al.* [81] introduced an SPRi sensor with polarisation contrast and a high-density array with low-fouling background. This sensor provided 120 channels for detection of ALCAM and hCG with respective concentrations of 45 and 100 ng/ml in 10% blood plasma samples. To control the levels of immobilisation during fabrication of the high-density array, a DNA-directed method was employed.

In the SPRi sensing demonstrations previously described, the limits of detection for hCG, ALCAM, and TAGLN-2 were below their clinically significant level. Recently, SPRi, in conjunction with an antibody-conjugated QD micropatterned chip, allowed the simultaneous detection of up to four biomarkers, i.e. Fas, angiopoietin 2 (Ang-2), human epidermal growth factor receptor 2 (HER-2), and matrix metallopeptidase-9 (MMP-9). Employing this sensor, Shabani and Tabrizian [82] demonstrated a limit of detection of 25 pg/ml in PBS, which is comparable with the concentration of most biomarkers in vivo. The high sensitivity achieved with this sensor is attributed to the QDs introduced in the surface chemistry. A more thorough discussion on QDs will be presented in Section 5.

The devices reviewed in this section have been demonstrated to achieve high-throughput screening of protein biomarkers in complex samples (e.g. blood plasma). Moreover, different antibody immobilisation strategies can be implemented to optimise the density of antibodies in the protein arrays. Additionally, the detection limits obtained with these high-throughput devices are comparable with those of low-throughput SPR sensors, making them a clinically feasible alternative to cancer biomarker detection.

4.5 Sandwich-type SPR

SPR systems have adopted the classical sandwich configuration of immunoassays as a strategy to improve their sensitivity. A sandwich-type SPR (sSPR) sensor consists of a capture primary antibody, a target antigen, and a labelled secondary antibody. In sSPR sensors, the primary antibody is typically immobilised to an SAM surface and the label type of the secondary antibody dictates the signal generation resulting from target antigen capture.

Jang *et al.* [83] developed an sSPR sensor based on a side-polished and Au-coated few-mode-fibre (FMF), which allowed the use of a low-cost halogen lamp without degrading its sensing performance because of improved coupling efficiency with the FMF. The work therein reported implies that the proposed sSPR sensor is capable of detecting a change in concentrations of prostate-specific antigen (PSA) in PBS at the nanogram-per-millilitre level. Another performance improvement strategy for sSPR-based sensors was recently introduced by Li *et al.* [84] in which Au nanoparticles modified with SA were used for signal amplification of an sSPR sensor, allowing to detect CEA in serum at a concentration of 1 ng/ml over the range of 1–60 ng/ml.

Nevertheless, from all these sSPR sensing demonstrations, only the limits of detection for alphafetoprotein antigen (AFP) and CEA were below their clinically significant level. Advantages of sSPR sensors include disposability, high sensitivity, simple fabrication, and label-free detection. These sensors have great potential for real-time analysis of the immune response between biomolecules, and can be employed in fields as diverse as chemical, biological, and environmental sensing, among others.

4.6 Localised SPR

A modern label-free approach to enhance sensitivity of SPR systems exploits noble metal nanostructures supporting localised SPR (LSPR) as a signal amplification strategy. LSPR is a near-field

Table 4 QDs-based sensing devices

Reference	Type of cancer	Targeted biomarker	Type of study	Type of QD	Solution
Fang et al. [96]	liver, gastric, breast, cervical	AB6586, MA1-38069, SC-20072	*in vitro*	prefabricated QDs (Invitrogen, USA)	N/A
Li et al. [97]	breast	MMP-2	*in vivo/ in vitro*	CdTe	PBS (for in vitro detection)
Rakovich et al. [98]	lung	HER-2	*in vitro*	Cd/ZnS QD conjugated to a single domain anti-HER2 antibodies (sdAbs)	DMEM, RPMI, and McCoy's 5A mediums
Kwon et al. [99]	breast	ER, PR, HER-2	*in vitro*	prefabricated QDs (Invitrogen, USA) visualised on CK	2% BSA, 5% goat serum, and PBS
Han et al. [100]	lung	EGFR, carcinoembryonic antigen-related cell adhesion molecule 1	*in vivo*	Au:CdHgTe	blood
Tan et al. [101]	liver	Ag nitrate and sodium sulphide as QDs precursors	*in vivo*	Ag_2S	blood

phenomenon (<20 nm) leading to sharp peaks in the extinction spectra of nanostructures; e.g. Au and silver (Ag) nanoparticles exhibit LSPR at optical wavelengths [86].

A first generation of parallel LSPR sensors focused on a simple periodic arrangement of Au nanorods immobilised on a glass substrate was introduced by Acimovic et al. in [85]. The sensor offered parallel, real-time inspection of 32 sensing sites distributed across eight independent microfluidic channels with very high reproducibility. Detection of AFP and PSA in 50% human serum was demonstrated down to concentrations of 500 pg/ml and 1 ng/ml, respectively. The corresponding linear ranges for AFP and PSA were determined to be between 5 and 1000 and 10 and 100 ng/ml. Similar LSPR sensors were used by Geng et al. [86] to detect AFP in PBS at a concentration of 25 ng/ml and by Hu et al. [88] to detect miRNA at single nanoparticle level with limit of detection up to 3 nM.

Sanders et al. [87] reported an LSPR-coupled fibre-optic (FO) nanoprobe for detecting free prostate-specific antigen (f-PSA) with a limit of detection at 100 fg/ml in PBS and linear range between 100 fg/ml and 5 ng/ml. In this approach, a low-cost, lift-off process was developed to fabricate Au nanodisk arrays at the end facet of a single-mode 4.3 μm diameter optical fibre (@633 nm), providing a great spectral stability over the range of 600−750 nm, in which the resonance peaks are typically located.

In all LSPR sensing demonstrations, the limits of detection for AFP, PSA, and f-PSA were below their clinically significant level. LSPR biosensors are label-free and can tackle a number of multiplexed sensing applications. They have the potential to become the next generation of point-of-care devices for early detection of cancer and many more diseases.

5 Cancer detection using QDs

Quantum crystallites or QDs with dimensions from 2 to 50 nm have been widely studied because of their special electromagnetic polariton size and quantum size effects. QDs are stable bright fluorophores that exhibit very long Stokes shifts and their operation-wavelength can be tailored based on their size and shape. In a QD, the quantum confinement effect occurs when the nanoparticle radius is lower than the Bohr radius of the electron, exciton, and hole. The diameter of a QD determines its bandgap and hence the colour of the light it emits, which can be fine-tuned by the choice of building material and core size [90].

QDs exhibit a range of attractive features, which can be exploited in sensing applications. For example, in contrast to organic dyes (ODs) widely used as fluorescence detection elements, when the excitation photons are in limited supply, QDs present a very broad absorption profile and a narrow wavelength emission-peak. Another advantage over ODs is its high quantum yield (QY). QDs can reach QYs above 60% in both visible and near-infrared region (NIR), whereas ODs present high QY in the visible region, but below 20% in the NIR region. Moreover, QDs allow sensitive separation between auto-fluorescence signals and scattered light

from excitation imaging signals. In the case of ODs for both visible and NIR regions, the fluorescence lifetimes are very short, causing difficulties for temporal discrimination between fluorescence interference and scattering from excitation signals [91]. Owing to these features, QDs have become a tool for the understanding of biological processes such as cancer metastasis. Though only a few research works on QDs-based sensing readily available in the literature employ microfluidic technologies to detect cancer cells/biomarkers, many of them employ microfluidic technologies for a range of disease diagnostics [92–95]. Therefore, we have included this section in our review as we consider it feasible that together, QDs and microfluidics, will soon allow developing highly sensitive and selective cancer detection platforms. In Table 4, we summarise the most recent development in cancer detection with QDs.

5.1 In vitro cancer detection

In vitro tests allow determining the disease progression as well as the different mechanism of cancer evolution. In a controlled frame, molecular interactions can be studied obtaining useful information about tumour microenvironment and cancer progression.

Fang et al. [96] studied the degradation, uncoiling, deposition, and modification of collagen-IV employing QDs. The extracellular matrix binds cells and tissues together, and collagens are among its major constituents, serving as effective barriers against cancer intrusions. Later, in 2014, Rakovich et al. [98] used QDs conjugated to a single domain antibody (sdAb) to detect a known cancer biomarker, the tyrosine kinase HER2 which is overexpressed in lung, uterine, breast, and stomach cancer. The study compared sdAb-QD against ODs. The detection of low expression levels of HER2 was demonstrated using confocal microscopy, concluding that QD conjugates show more sensitivity and specificity than their OD counterparts.

The use of QDs in the detection of multiple cancer biomarkers has also been reported. Parallel biomarker detection is required in both study and diagnosis of cancer. Kwon et al., in [99], described a concept for detection and quantification of the expression of estrogen receptor (ER), progesterone receptor (PR) and HER2 in breast cancer tissue using QDs. Parallel detection was achieved using a CK-based tumour-specific antigenic-site selection strategy. A microfluidic device was fabricated to incubate antibodies for each biomarker and functionalise QDs in rectangular microchannels. Then, on mixing of the conjugated QDs with the sample, QD excitation and visualisation was carried out. The thus obtained biomarker intensities correlated well against the results of conventional scoring techniques (e.g. immunohistochemistry test).

5.2 In vivo cancer detection

When using QDs based in vivo detection, imaging and infiltration pose a major challenge due to their high toxicity. A series of workarounds have already been tested to minimise damage to

neighbouring cells, nevertheless, further research is still required for QD to safely interact with living cells.

Han *et al.* reported the use of mercury cadmium telluride (CdHgTe)-NIR QDs doped with Au in order to enhance photoluminescence and decrease cytotoxicity in [100]. Such modified QDs served successfully as bioprobes for lung cancer cell multispectral-fluorescence-imaging (MSFI), which captures fluorescence image data at different spectral frequencies. In traditional in vivo fluorescence, the emission spectra may overlap significantly for signals of biological interest. Also, those signals may be obscured by auto-fluorescence of the animal tissue. MSFI solves this problem by using full imaging over a wide range of optical frequencies. The thus obtained fluorescence signals from QDs bioconjugates were then employed to detect three tumour markers in four week old male nude mice.

In [97], Li *et al.* described the use of QDs to detect matrix metalloproteinase-2 (MMP-2), a protease related to metastasis and tumourigenesis. Since MMP-2 is highly secreted by malignant tumour cells, it constitutes an attractive biomarker for cancer detection. In this paper, the tumour models were injected in nude mice and QD were administered to the tumour via intratumoural injection. With this approach, the MMP-2 activity was successfully monitored in vivo.

5.3 Toxicity

Most QDs are fabricated from cadmium selenide or telluride. Cadmium ions stress and damage cells, and therefore constitute the primary cause of QDs cytotoxicity. In addition, QDs with heavy metals also affect the normal cell activity and damage DNA. Nonetheless, surface functionalisation has been found to reduce nanoparticle cytotoxicity [90]. Suitable QDs for in vivo monitoring include, but are not limited to: CdHgTe, cadmium telluride/cadmium selenide (CdTe/CdSe), indium arsenide/indium phosphide/zinc selenide, copper indium selenide, and cadmium arsenide [100].

Carbon QDs (CQDs), an alternative to semiconductor-based QDs, exhibit low toxicity, good biocompatibility, similar optical properties, and low cost of production as they can be synthesised via inexpensive and synthetic routes. Moreover, CQDs also feature tuneable emissions, but they usually exhibit low QY. To tackle this problem, surface passivation with organic or polymeric materials has been used, resulting in strong fluorescence emissions. Furthermore, CQDs can be used as nanocarriers to track and deliver drugs to very specific sites [102].

Synthesis of QDs with biocompatible materials has been explored for their use as fluorescent probes in the NIR region for live animal imaging. Tan *et al.* [101] employed Ag sulphide (Ag$_2$S) nanocrystals to provide images with high contrast, which resulted from the deep tissue penetration. The Ag nitrate and sodium sulphide precursors were internalised by cultured cancer cells. According to this paper, the endogenous reduced glutathione (GSH) in cells favours the intracellular formation of Ag$_2$S QDs strongly.

6 Conclusion

In this review paper, we have summarised the most recent developments in microfluidic devices for cells/biomarkers manipulation and detection, focusing our attention to four different microfluidic sub-categories, i.e. immunomagnetic-affinity-based microfluidics, dielectrophoretically driven microfluidics, SPR micro-fluidic sensors, and QDs-based sensors. Immunomagnetic-affinity manipulation of cells and DEP represent excellent methods to enrich CTCs from a sample, while SPR- and QDs-based sensors exhibit an important degree of flexibility for multiplexed sample screening.

The performance of devices reviewed herein was characterised through different metrics (capture efficiency, capture purity, and limit of detection, among others) from which we can conclude that both, immunomagnetic-affinity-based and DEP-based, cell-sorting approaches can feature very high capture efficiencies (>90%) for a wide range of cancer cell lines and can work directly with blood samples. Nevertheless, though the fabrication of some dielectrophoretic devices (iDEP or cDEP) is rather inexpensive (in many cases cheaper than their immunomagnetic-affinity counterparts), they require more expensive external equipment to operate (e.g. costly power sources). On the other hand, DEP is a label-free technique that manipulates the cells as a function of their dielectric properties, a trait not available in immunomagnetic-affinity-based cell sorters. Furthermore, in the case of immunomagnetic-affinity-based sorters, it is important to characterise the particles employed as labels to achieve reproducibility in the experiments, adding complexity to the overall process. An attractive feature of both techniques is that they can be integrated into point-of-care screening platforms featuring a detection chamber, where detection can be carried out through electrochemical methods. Immunomagnetic-affinity-based and dielectrophoretic-based cell sorters exhibit a wide range of maximum operational sample flow rates, which in some cases significantly limits sample throughput. This is due to several different factors including channel geometry, stiffness of embedded structures, and adhesion of the channel to the substrate, among others. Perhaps the most influential reason is the device geometry. Wider and taller channels allow for higher flow rates. In particular, for the case of immunomagnetic-affinity-based microfluidic devices with embedded structures, the stiffness of such structures may also limit the maximum operational flow rate. In the case of DEP-based cell-sorters, owing to the important 3D distortion they exert on the electric field distribution within the channel, iDEP and cDEP devices present the highest flow rates.

In the case of the SPR-based and QD-based sensing platforms, both approaches can lead to selective detection of cells, as both of them rely on immunoaffinity-based interactions. Nevertheless, the amount of research works reported for SPR-based microfluidic sensing platforms outnumbers that for QDs-based methods. One reason for this may be the high toxicity trait in QDs. Though from this perspective SPR-based sensing platforms seem to be the best option with limits of detection in the order of fg/ml, the technology is very expensive. We foresee that, with the introduction of CQDs and advances in microfluidic technology, CQDs-based cancer cell detection might become an attractive alternative to costly SPR-based methods.

7 Acknowledgment

8 References

1   Dong, Y., Skelley, A.M., Merdek, K.D., *et al.*: 'Microfluidics and circulating tumor cells', *J. Mol. Diagn.*, 2013, **15**, (2), pp. 149–157
2   Chaffer, C.L., Weinberg, R.A.: 'A perspective on cancer cell metastasis', *Science*, 2011, **331**, (6024), pp. 1559–1564
3   McPherson, R.A., Pincus, M.R.: 'Henry's clinical diagnosis and management by laboratory methods' (Elsevier Health Sciences, 2011)
4   Yu, M., Stott, S., Toner, M., *et al.*: 'Circulating tumor cells: approaches to isolation and characterization', *J. Cell Biol.*, 2011, **192**, (3), pp. 373–382
5   Squires, T.M., Quake, S.R.: 'Microfluidics: fluid physics at the nanoliter scale', *Rev. Mod. Phys.*, 2005, **77**, (3), p. 977
6   Augustsson, P., Magnusson, C., Nordin, M., *et al.*: 'Microfluidic, label-free enrichment of prostate cancer cells in blood based on acoustophoresis', *Anal. Chem.*, 2012, **84**, (18), pp. 7954–7962
7   Bhagat, A.A.S., Hou, H.W., Li, L.D., *et al.*: 'Pinched flow coupled shear-modulated inertial microfluidics for high-throughput rare blood cell separation', *Lab Chip*, 2011, **11**, (11), pp. 1870–1878
8   Burger, R., Kirby, D., Glynn, M., *et al.*: 'Centrifugal microfluidics for cell analysis', *Curr. Opin. Chem. Biol.*, 2012, **16**, (3–4), pp. 409–414
9   Chen, J., Li, J., Sun, Y.: 'Microfluidic approaches for cancer cell detection, characterization, and separation', *Lab Chip*, 2012, **12**, (10), pp. 1753–1767
10 Qian, W., Zhang, Y., Chen, W.: 'Capturing cancer: emerging microfluidic technologies for the capture and characterization of circulating tumor cells', *Small*, 2015, **11**, (32), pp. 3850–3872

11 Castro, C.M., Ghazani, A.A., Chung, J., *et al.*: 'Miniaturized nuclear magnetic resonance platform for detection and profiling of circulating tumor cells', *Lab Chip*, 2014, **14**, (1), pp. 14–23

12 Hejazian, M., Li, W., Nguyen, N.-T.: 'Lab on a chip for continuous-flow magnetic cell separation', *Lab Chip*, 2015, **15**, (4), pp. 959–970

13 Hoshino, K., Huang, Y.-Y., Lane, N., *et al.*: 'Microchip-based immunomagnetic detection of circulating tumor cells', *Lab Chip*, 2011, **11**, (20), pp. 3449–3457

14 Forbes, T.P., Forry, S.P.: 'Microfluidic magnetophoretic separations of immunomagnetically labeled rare mammalian cells', *Lab Chip*, 2012, **12**, (8), pp. 1471–1479

15 Banerjee, S.S., Jalota-Badhwar, A., Satavalekar, S.D., *et al.*: 'Transferrin – mediated rapid targeting, isolation, and detection of circulating tumor cells by multifunctional magneto – dendritic nanosystem', *Adv. Healthc. Mater.*, 2013, **2**, (6), pp. 800–805

16 Huang, Y.-Y., Hoshino, K., Chen, P., *et al.*: 'Immunomagnetic nanoscreening of circulating tumor cells with a motion controlled microfluidic system', *Biomed. Microdevices*, 2013, **15**, (4), pp. 673–681

17 Wu, C.-H., Huang, Y.-Y., Chen, P., *et al.*: 'Versatile immunomagnetic nanocarrier platform for capturing cancer cells', *ACS Nano*, 2013, **7**, (10), pp. 8816–8823

18 Han, N., Shin, J.H., Han, K.-H.: 'An on-chip RT-PCR microfluidic device, that integrates MRNA extraction, CDNA synthesis, and gene amplification', *RSC Adv.*, 2014, **4**, (18), pp. 9160–9165

19 Liu, X., Wang, X., Wu, X., *et al.*: 'The synergistic effect of periodic immunomagnetics and microfluidics on universally capturing circulating tumor cells', *Microsyst. Technol.*, 2014, **20**, (7), pp. 1337–1344

20 Watanabe, M., Serizawa, M., Sawada, T., *et al.*: 'A novel flow cytometry-based cell capture platform for the detection, capture and molecular characterization of rare tumor cells in blood', *J. Translational Med.*, 2014, **12**, (1), p. 143

21 Horak, D., Svobodova, Z., Autebert, J., *et al.*: 'Albumin – coated monodisperse magnetic poly (glycidyl methacrylate) microspheres with immobilized antibodies: application to the capture of epithelial cancer cells', *J. Biomed. Mater. Res. A*, 2013, **101**, (1), pp. 23–32

22 Earhart, C.M., Hughes, C.E., Gaster, R.S., *et al.*: 'Isolation and mutational analysis of circulating tumor cells from lung cancer patients with magnetic sifters and biochips', *Lab Chip*, 2014, **14**, (1), pp. 78–88

23 Autebert, J., Coudert, B., Champ, J., *et al.*: 'High purity microfluidic sorting and analysis of circulating tumor cells: towards routine mutation detection', *Lab Chip*, 2015, **15**, (9), pp. 2090–2101

24 Wang, C., Ye, M., Cheng, L., *et al.*: 'Simultaneous isolation and detection of circulating tumor cells with a microfluidic silicon-nanowire-array integrated with magnetic upconversion nanoprobes', *Biomaterials*, 2015, **54**, pp. 55–62

25 Kang, J.H., Krause, S., Tobin, H., *et al.*: 'A combined micromagnetic-microfluidic device for rapid capture and culture of rare circulating tumor cells', *Lab Chip*, 2012, **12**, (12), pp. 2175–2181

26 Ozkumur, E., Shah, A.M., Ciciliano, J.C., *et al.*: 'Inertial focusing for tumor antigen-dependent and -independent sorting of rare circulating tumor cells', *Sci. Translational Med.*, 2013, **5**, (179), p. 179ra147

27 Karabacak, N.M., Spuhler, P.S., Fachin, F., *et al.*: 'Microfluidic, marker-free isolation of circulating tumor cells from blood samples', *Nat. Protocols*, 2014, **9**, (3), pp. 694–710

28 Hyun, K.-A., Lee, T.Y., Lee, S.H., *et al.*: 'Two-stage microfluidic chip for selective isolation of circulating tumor cells (CTCS)', *Biosens. Bioelectron.*, 2015, **67**, pp. 86–92

29 Kirby, D., Glynn, M., Kijanka, G., *et al.*: 'Rapid and cost – efficient enumeration of rare cancer cells from whole blood by low – loss centrifugo – magnetophoretic purification under stopped-flow conditions', *Cytometry A*, 2015, **87**, (1), pp. 74–80

30 Mohamadi, R.M., Besant, J.D., Mepham, A., *et al.*: 'Nanoparticle-mediated binning and profiling of heterogeneous circulating tumor cell subpopulations', *Angew. Chem. Int. Ed.*, 2015, **54**, (1), pp. 139–143

31 Malhotra, R., Patel, V., Chikkaveeraiah, B.V., *et al.*: 'Ultrasensitive detection of cancer biomarkers in the clinic by use of a nanostructured microfluidic array', *Anal. Chem.*, 2012, **84**, (14), pp. 6249–6255

32 Bettazzi, F., Hamid-Asl, E., Esposito, C.L., *et al.*: 'Electrochemical detection of miRNA-222 by use of a magnetic bead-based bioassay', *Anal. Bioanal. Chem.*, 2013, **405**, (2–3), pp. 1025–1034

33 Zitka, O., Cernei, N., Heger, Z., *et al.*: 'Microfluidic chip coupled with modified paramagnetic particles for sarcosine isolation in urine', *Electrophoresis*, 2013, **34**, (18), pp. 2639–2647

34 Lee, T.Y., Shin, Y., Park, M.K.: 'A simple, low-cost, and rapid device for a DNA methylation-specific amplification/detection system using a flexible plastic and silicon complex', *Lab Chip*, 2014, **14**, (21), pp. 4220–4229

35 Otieno, B.A., Krause, C.E., Latus, A., *et al.*: 'On-line protein capture on magnetic beads for ultrasensitive microfluidic immunoassays of cancer biomarkers', *Biosens. Bioelectron.*, 2014, **53**, pp. 268–274

36 Lin, Y.-H., Peng, P.-Y.: 'Semiconductor sensor embedded microfluidic chip for protein biomarker detection using a bead-based immunoassay combined with deoxyribonucleic acid strand labeling', *Anal. Chim. Acta*, 2015, **869**, pp. 34–42

37 Hughes, M.P.: 'Nanoelectromechanics in engineering and biology' (CRC Press, 2002)

38 Pohl, H.A.: 'The motion and precipitation of suspensoids in divergent electric fields', *J. Appl. Phys.*, 1951, **22**, (7), pp. 869–871

39 Kirby, B.J.: 'Micro- and nanoscale fluid mechanics. Transport in microfluidic devices' (Cambridge University Press, 2010)

40 Pethig, R.: 'Review article – dielectrophoresis: status of the theory, technology, and applications', *Biomicrofluidics*, 2010, **4**, (2), p. 022811

41 Washizu, M., Kurosawa, O.: 'Electrostatic manipulation of DNA in microfabricated structures', *IEEE Trans. Ind. Appl.*, 1990, **26**, (6), pp. 1165–1172

42 Cummings, E.B., Singh, A.K.: 'Dielectrophoresis in microchips containing arrays of insulating posts: theoretical and experimental results', *Anal. Chem.*, 2003, **75**, (18), pp. 4724–4731

43 Gascoyne, P., Huang, Y., Pethig, R., *et al.*: 'Dielectrophoretic separation of mammalian cells studied by computerized image analysis', *Meas. Sci. Technol.*, 1992, **3**, (5), p. 439

44 Moon, H.-S., Kwon, K., Kim, S.-I., *et al.*: 'Continuous separation of breast cancer cells from blood samples using multi-orifice flow fractionation (Moff) and dielectrophoresis (Dep)', *Lab Chip*, 2011, **11**, (6), pp. 1118–1125

45 Mulhall, H.J., Labeed, F.H., Kazmi, B., *et al.*: 'Cancer, pre-cancer and normal oral cells distinguished by dielectrophoresis', *Anal. Bioanal. Chem.*, 2011, **401**, (8), pp. 2455–2463

46 Gupta, V., Jafferji, I., Garza, M., *et al.*: 'Apostream(™), a new dielectrophoretic device for antibody independent isolation and recovery of viable cancer cells from blood', *Biomicrofluidics*, 2012, **6**, (2), p. 024133

47 Wu, L., Yung, L.-Y.L., Lim, K.-M.: 'Dielectrophoretic capture voltage spectrum for measurement of dielectric properties and separation of cancer cells', *Biomicrofluidics*, 2012, **6**, (1), p. 014113

48 Fabbri, F., Carloni, S., Zoli, W., *et al.*: 'Detection and recovery of circulating colon cancer cells using a dielectrophoresis-based device: KRAS mutation status in pure CTCS', *Cancer Lett.*, 2013, **335**, (1), pp. 225–231

49 Huang, C., Santana, S.M., Liu, H., *et al.*: 'Characterization of a hybrid dielectrophoresis and immunocapture microfluidic system for cancer cell capture', *Electrophoresis*, 2013, **34**, (20–21), pp. 2970–2979

50 Huang, C., Liu, H., Bander, N., *et al.*: 'Enrichment of prostate cancer cells from blood cells with a hybrid dielectrophoresis and immunocapture microfluidic system', *Biomed. Microdevices*, 2013, **15**, (6), pp. 941–948

51 Huang, C., Smith, J.P., Saha, T.N., *et al.*: 'Characterization of microfluidic shear-dependent epithelial cell adhesion molecule immunocapture and enrichment of pancreatic cancer cells from blood cells with dielectrophoresis', *Biomicrofluidics*, 2014, **8**, (4), p. 044107

52 Bhattacharya, S., Chao, T.-C., Ros, A.: 'Insulator-based dielectrophoretic single particle and single cancer cell trapping', *Electrophoresis*, 2011, **32**, (18), pp. 2550–2558

53 Bhattacharya, S., Chao, T.-C., Ariyasinghe, N., *et al.*: 'Selective trapping of single mammalian breast cancer cells by insulator-based dielectrophoresis', *Anal. Bioanal. Chem.*, 2014, **406**, (7), pp. 1855–1865

54 Smith, J.P., Huang, C., Kirby, B.J.: 'Enhancing sensitivity and specificity in rare cell capture microdevices with dielectrophoresis', *Biomicrofluidics*, 2015, **9**, (1), p. 014116

55 Henslee, E.A., Sano, M.B., Rojas, A.D., *et al.*: 'Selective concentration of human cancer cells using contactless dielectrophoresis', *Electrophoresis*, 2011, **32**, (18), pp. 2523–2529

56 Sano, M.B., Caldwell, J.L., Davalos, R.V.: 'Modeling and development of a low frequency contactless dielectrophoresis (CDEP) platform to sort cancer cells from dilute whole blood samples', *Biosens. Bioelectron.*, 2011, **30**, pp. 13–20

57 Sano, M.B., Henslee, E.A., Schmelz, E., *et al.*: 'Contactless dielectrophoretic spectroscopy: examination of the dielectric properties of cells found in blood', *Electrophoresis*, 2011, **32**, (22), pp. 3164–3171

58 Salmanzadeh, A., Romero, L., Shafiee, H., *et al.*: 'Isolation of prostate tumor initiating cells (Tics) through their dielectrophoretic signature', *Lab Chip*, 2012, **12**, (1), pp. 182–189

59 Salmanzadeh, A., Kittur, H., Sano, M.B., *et al.*: 'Dielectrophoretic differentiation of mouse ovarian surface epithelial cells, macrophages, and fibroblasts using contactless dielectrophoresis', *Biomicrofluidics*, 2012, **6**, (2), pp. 024104–024113

60 Sano, M.B., Salmanzadeh, A., Davalos, R.V.: 'Multilayer contactless dielectrophoresis: theoretical considerations', *Electrophoresis*, 2012, **33**, (13), pp. 1938–1946

61 Salmanzadeh, A., Sano, M.B., Gallo-Villanueva, R.C., *et al.*: 'Investigating dielectric properties of different stages of syngeneic murine ovarian cancer cells', *Biomicrofluidics*, 2013, **7**, (1), p.011809

62 Demircan, Y., Koyuncuoğlu, A., Erdem, M., *et al.*: 'Label-free detection of multidrug resistance in K562 cells through isolated 3d-electrode dielectrophoresis', *Electrophoresis*, 2015, **36**, (9–10), pp. 1149–1157

63 Wang, L., Lu, J., Marchenko, S.A., *et al.*: 'Dual frequency dielectrophoresis with interdigitated sidewall electrodes for microfluidic flow-through separation of beads and cells', *Electrophoresis*, 2009, **30**, (5), pp. 782–791

64 Xiaoxing, X., Mengying, Z., Yobas, L.: 'Interdigitated 3-D silicon ring microelectrodes for dep-based particle manipulation', *J. Microelectromech. Syst.*, 2013, **22**, (2), pp. 363–371

65 Jia, Y., Ren, Y., Jiang, H.: 'Continuous dielectrophoretic particle separation using a microfluidic device with 3d electrodes and vaulted obstacles', *Electrophoresis*, 2015, **36**, (15), pp. 1744–1753

66 Martinez-Duarte, R., Renaud, P., Madou, M.J.: 'A novel approach to dielectrophoresis using carbon electrodes', *Electrophoresis*, 2011, **32**, (17), pp. 2385–2392

67 Perez-Gonzalez, V.H., Ho, V., Kulinsky, L., *et al.*: 'PPyDEP: a new approach to microparticle manipulation employing polymer-based electrodes', *Lab Chip*, 2013, **13**, (23), pp. 4642–4652

68 Becker, F.F., Wang, X.B., Huang, Y., *et al.*: 'Separation of human breast cancer cells from blood by differential dielectric affinity', *Proc. Natl. Acad. Sci. USA*, 1995, **92**, (3), pp. 860–864

69 Becker, F.F., Wang, X.-B., Huang, Y., *et al.*: 'The removal of human leukaemia cells from blood using interdigitated microelectrodes', *J. Phys. D, Appl. Phys.*, 1994, **27**, (12), p. 2659

70 Han, K.N., Li, C.A., Seong, G.H.: 'Microfluidic chips for immunoassays', in Cooks, R.G., Pemberton, J.E. (Eds.): 'Annual review of analytical chemistry' (Annual Reviews, 2013), vol. 6

71 Homola, J.: 'Surface plasmon resonance based sensors', *Surf. Plasmon Reson. Based Sens.*, 2006, **4**, pp. 1–251

72 Choi, S., Chae, J.: 'A microfluidic biosensor based on competitive protein adsorption for thyroglobulin detection', *Biosens. Bioelectron.*, 2009, **25**, (1), pp. 118–123

73 Chang, C.C., Chiu, N.F., Lin, D.S., *et al.*: 'High-sensitivity detection of carbohydrate antigen 15-3 using a gold/zinc oxide thin film surface plasmon resonance-based biosensor', *Anal. Chem.*, 2010, **82**, (4), pp. 1207–1212

74 Chen, H.X., Hou, Y.F., Qi, F.J., *et al.*: 'Detection of vascular endothelial growth factor based on rolling circle amplification as a means of signal enhancement in surface plasmon resonance', *Biosens. Bioelectron.*, 2014, **61**, pp. 83–87

75 Jang, D.H., Choi, Y., Choi, Y.S., *et al.*: 'Sensitive and selective analysis of a wide concentration range of Igfbp7 using a surface plasmon resonance biosensor', *Colloids Surf. B, Biointerfaces*, 2014, **123**, pp. 887–891

76 Ladd, J., Lu, H.L., Taylor, A.D., *et al.*: 'Direct detection of carcinoembryonic antigen autoantibodies in clinical human serum samples using a surface plasmon resonance sensor', *Colloids Surf. B, Biointerfaces*, 2009, **70**, (1), pp. 1–6

77 Fang, X.Y., Tie, J., Xie, Y.H., *et al.*: 'Detection of gastric carcinoma-associated antigen Mg7-Ag in human sera using surface plasmon resonance sensor', *Cancer Epidemiol.*, 2010, **34**, (5), pp. 648–651

78 Springer, T., Piliarik, M., Homola, J.: 'Real-time monitoring of biomolecular interactions in blood plasma using a surface plasmon resonance biosensor', *Anal. Bioanal. Chem.*, 2010, **398**, (5), pp. 1955–1961

79 Law, W.C., Yong, K.T., Baev, A., *et al.*: 'Sensitivity improved surface plasmon resonance biosensor for cancer biomarker detection based on plasmonic enhancement', *ACS Nano*, 2011, **5**, (6), pp. 4858–4864

80 Ladd, J., Taylor, A.D., Piliarik, M., *et al.*: 'Label-free detection of cancer biomarker candidates using surface plasmon resonance imaging', *Anal. Bioanal. Chem.*, 2009, **393**, (4), pp. 1157–1163

81 Piliarik, M., Bockova, M., Homola, J.: 'Surface plasmon resonance biosensor for parallelized detection of protein biomarkers in diluted blood plasma', *Biosens. Bioelectron.*, 2010, **26**, (4), pp. 1656–1661

82 Shabani, A., Tabrizian, M.: 'Design of a universal biointerface for sensitive, selective, and multiplex detection of biomarkers using surface plasmon resonance imaging', *Analyst*, 2013, **138**, (20), pp. 6052–6062

83 Jang, H.S., Park, K.N., Kang, C.D., *et al.*: 'Optical fiber SPR biosensor with sandwich assay for the detection of prostate specific antigen', *Opt. Commun.*, 2009, **282**, (14), pp. 2827–2830

84 Li, R., Feng, F., Chen, Z.-Z., *et al.*: 'Sensitive detection of carcinoembryonic antigen using surface plasmon resonance biosensor with gold nanoparticles signal amplification', *Talanta*, 2015, **140**, (0), pp. 143–149

85 Acimovic, S.S., Ortega, M.A., Sanz, V., *et al.*: 'LSPR chip for parallel, rapid, and sensitive detection of cancer markers in serum', *Nano Lett.*, 2014, **14**, (5), pp. 2636–2641

86 Geng, Z.X., Kan, Q., Yuan, J., *et al.*: 'A route to low-cost nanoplasmonic biosensor integrated with optofluidic-portable platform', *Sens. Actuators B, Chem.*, 2014, **195**, pp. 682–691

87 Sanders, M., Lin, Y.B., Wei, J.J., *et al.*: 'An enhanced LSPR fiber-optic nanoprobe for ultrasensitive detection of protein biomarkers', *Biosens. Bioelectron.*, 2014, **61**, pp. 95–101

88 Hu, Y.L., Zhang, L., Zhang, Y., *et al.*: 'Plasmonic nanobiosensor based on hairpin DNA for detection of trace oligonucleotides biomarker in cancers', *ACS Appl. Mater. Interfaces*, 2015, **7**, (4), pp. 2459–2466

89 Rapp, B.E., Gruhl, F.J., Lange, K.: 'Biosensors with label-free detection designed for diagnostic applications', *Anal. Bioanal. Chem.*, 2010, **398**, (6), pp. 2403–2412

90 Drbohlavova, J., Adam, V., Kizek, R., *et al.*: 'Quantum dots – characterization, preparation and usage in biological systems', *Int. J. Mol. Sci.*, 2009, **10**, (2), pp. 656–673

91 Cheng, X., Lowe, S.B., Reece, P.J., *et al.*: 'Colloidal silicon quantum dots: from preparation to the modification of self-assembled monolayers (SAMS) for bio-applications', *Chem. Soc. Rev.*, 2014, **43**, (8), pp. 2680–2700

92 Klostranec, J.M., Xiang, Q., Farcas, G.A., *et al.*: 'Convergence of quantum dot barcodes with microfluidics and signal processing for multiplexed high-throughput infectious disease diagnostics', *Nano Lett.*, 2007, **7**, (9), pp. 2812–2818

93 Zhang, H., Xu, T., Li, C.-W., *et al.*: 'A microfluidic device with microbead array for sensitive virus detection and genotyping using quantum dots as fluorescence labels', *Biosens. Bioelectron.*, 2010, **25**, (11), pp. 2402–2407

94 Kim, Y.-G., Moon, S., Kuritzkes, D.R., *et al.*: 'Quantum dot-based HIV capture and imaging in a microfluidic channel', *Biosens. Bioelectron.*, 2009, **25**, (1), pp. 89–96

95 Zhang, H., Liu, L., Li, C.-W., *et al.*: 'Multienzyme-nanoparticles amplification for sensitive virus genotyping in microfluidic microbeads array using Au nanoparticle probes and quantum dots as labels', *Biosens. Bioelectron.*, 2011, **29**, (1), pp. 89–96

96 Fang, M., Yuan, J.P., Peng, C.W., *et al.*: 'Quantum dots-based in situ molecular imaging of dynamic changes of collagen IV during cancer invasion', *Biomaterials*, 2013, **34**, (34), pp. 8708–8717

97 Li, X., Deng, D., Xue, J., *et al.*: 'Quantum dots based molecular beacons for in vitro and in vivo detection of MMP-2 on tumor', *Biosens. Bioelectron.*, 2014, **61**, pp. 512–518

98 Rakovich, T.Y., Mahfoud, O.K., Mohamed, B.M., *et al.*: 'Highly sensitive single domain antibody-quantum dot conjugates for detection of Her2 biomarker in lung and breast cancer cells', *ACS Nano*, 2014, **8**, (6), pp. 5682–5695

99 Kwon, S., Cho, C.H., Park, J.K., *et al.*: 'Automated measurement of multiple cancer biomarkers using quantum-dot-based microfluidic immunohistochemistry', *Anal. Chem.*, 2015, **87**, (8), pp. 4177–4183

100 Han, S., Mu, Y., Zhu, Q., *et al.*: 'Au:CdHgTe quantum dots for in vivo tumor-targeted multispectral fluorescence imaging', *Anal. Bioanal. Chem.*, 2012, **403**, (5), pp. 1343–1352

101 Tan, L., Wan, A., Li, H.: 'Synthesis of near-infrared quantum dots in cultured cancer cells', *ACS Appl. Mater. Interfaces*, 2014, **6**, (1), pp. 18–23

102 Lim, S.Y., Shen, W., Gao, Z.: 'Carbon quantum dots and their applications', *Chem. Soc. Rev.*, 2015, **44**, (1), pp. 362–381